PNAS
www.pnas.org

Supplementary Information for

Bending-torsional elasticity and energetics of the plus-end microtubule tip

Maxim Igaev and Helmut Grubmüller

Corresponding Authors.
E-mail: migaev@mpinat.mpg.de, hgrubmu@gwdg.de

This PDF file includes:

Figs. S1 to S10 (not allowed for Brief Reports)
Legends for Movies S1 to S3
Legends for Dataset S1 to S2

Other supplementary materials for this manuscript include the following:

Movies S1 to S3
Datasets S1 to S2

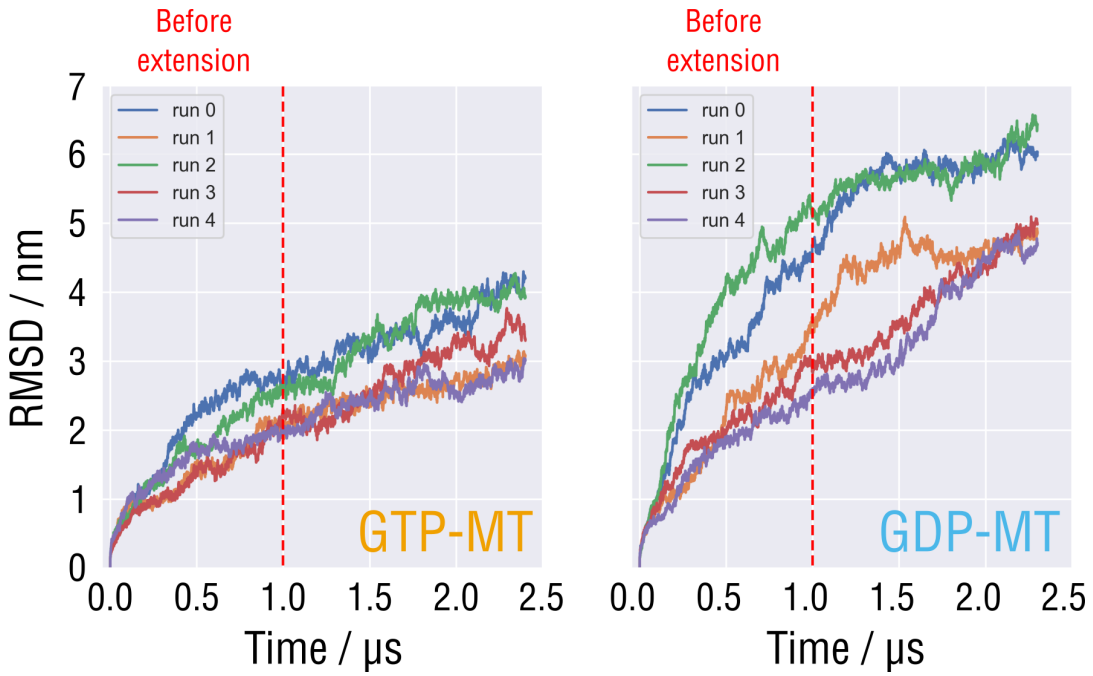

Fig. S1. Root mean square deviation (RMSD) of the relaxing MT tip structure from the initial straight conformation for each independent run and in each nucleotide state. The plot also includes the RMSD data collected in the extended simulations (beyond the red dashed line). The MT relaxation trajectories were stored every 125000 steps (500 ps). The time-resolved RMSD values were calculated relative to the starting straight configuration shown in Fig. 1*B* using the GROMACS internal tool `gmx rms`.

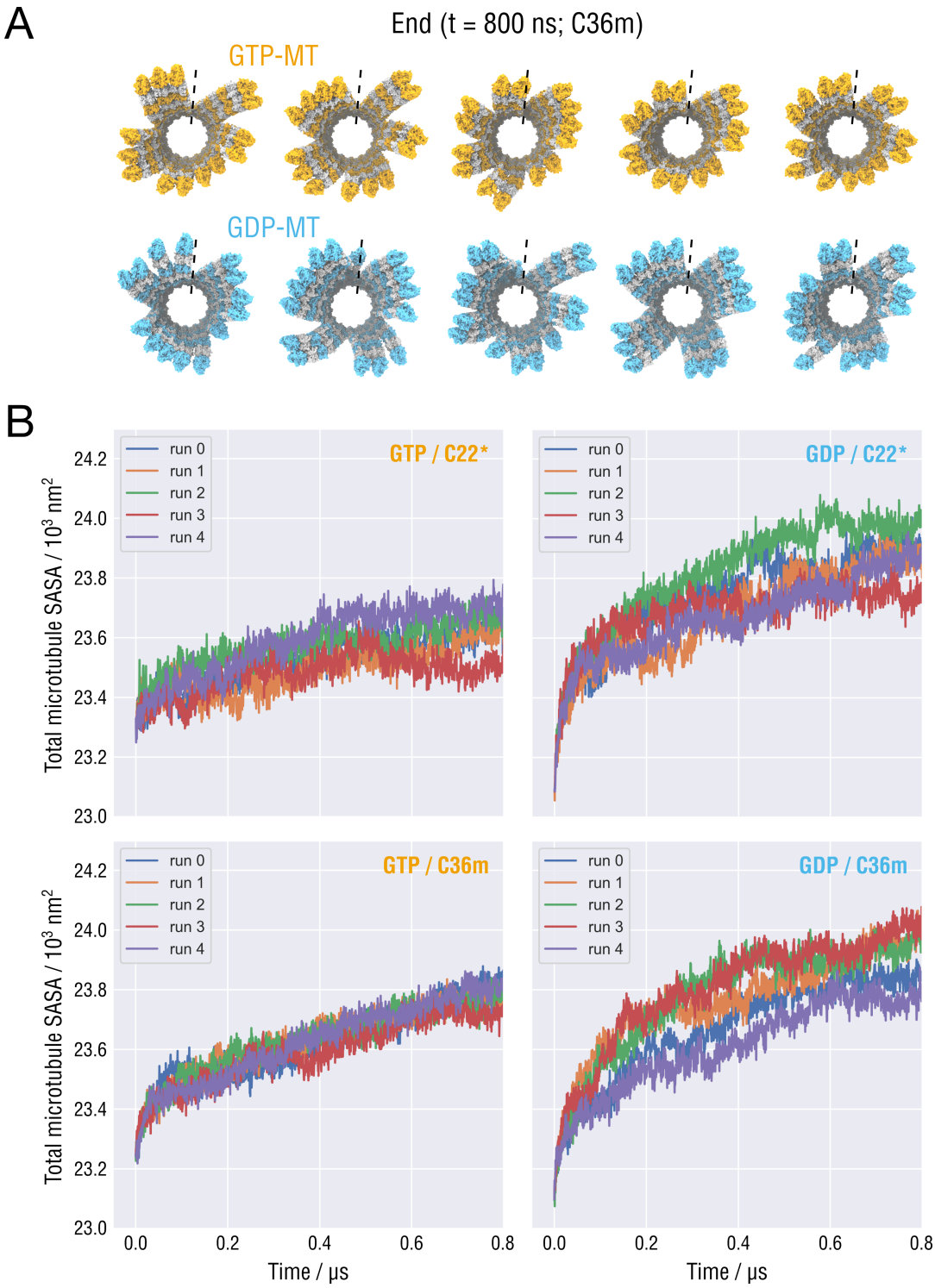

Fig. S2. (A) Splaying relaxation of the MT plus-end tip simulated with the CHARMM36m force field. Top view of the GTP- (orange) and GDP-MT (blue) tip structures after 800 ns of simulation. The seams are indicated with dashed lines. **(B)** Time evolution of the total MT SASA calculated using the CHARMM22* (top row) and CHARMM36m (bottom row) MT tip relaxation simulations.

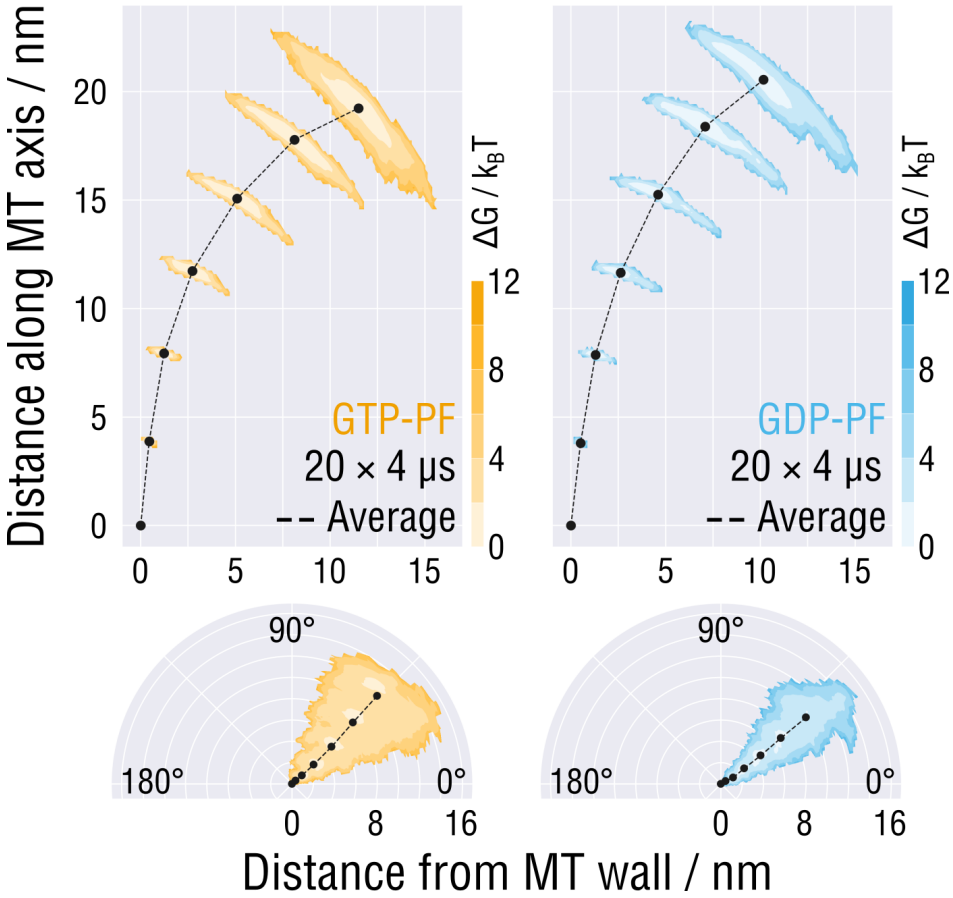

Fig. S3. Equilibrium distributions of the PF traces aligned with respect to the first minus-end monomers and projected onto the radial (top row) and transversal (bottom row) planes.

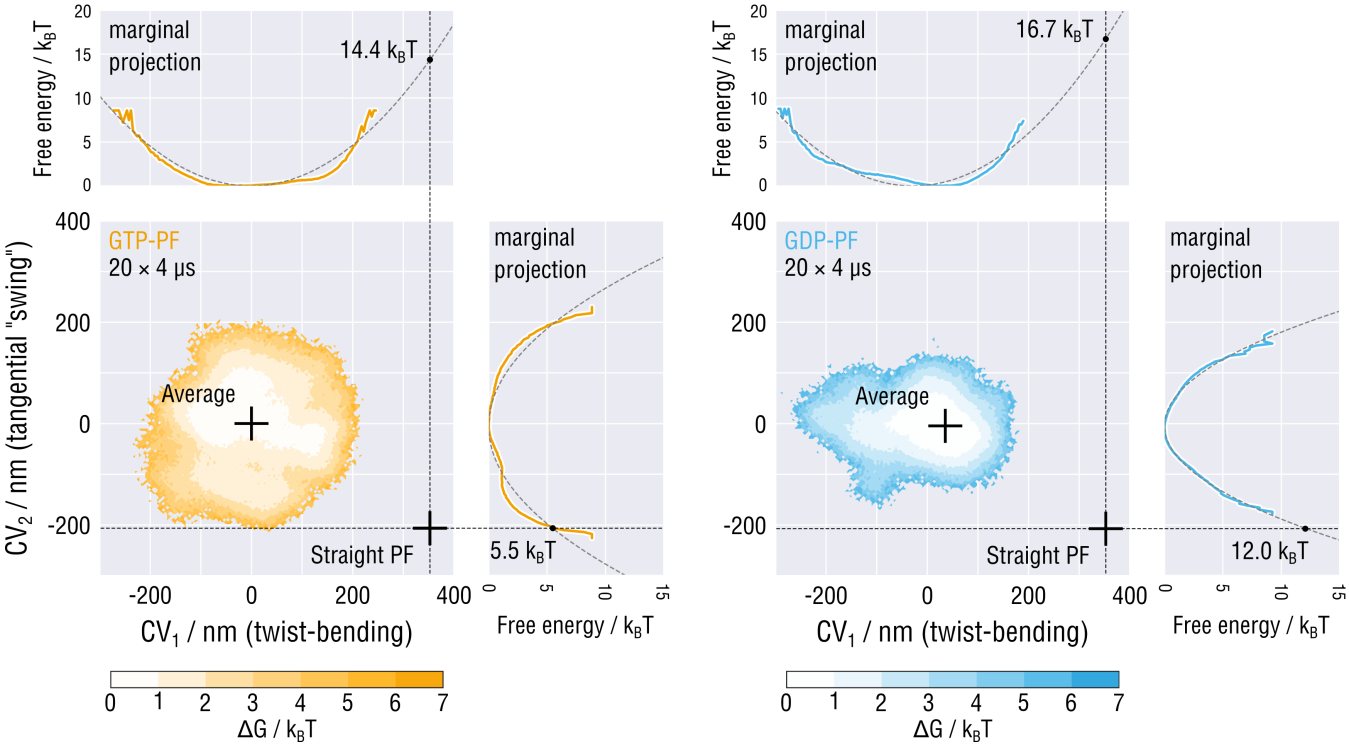

Fig. S4. One-dimensional marginal projections of the free energy profiles in Fig. 2A with the corresponding harmonic fits to illustrate the goodness of fit. The marginal profiles are rather smooth and – to a first approximation – followed the harmonic law. Among all projections, the marginal free energy profile along CV_2 for the GDP-PF is almost perfectly harmonic. The other fits, which do not fit that well, seem to have higher-order (*e.g.*, cubic) components such that the harmonic fit likely rather underestimates the free energy stored in the PF deformation and, therefore, provides conservative estimates. Given the achieved cumulative sampling of ~ 80 μs per nucleotide state, we consider this extrapolation sufficiently accurate.

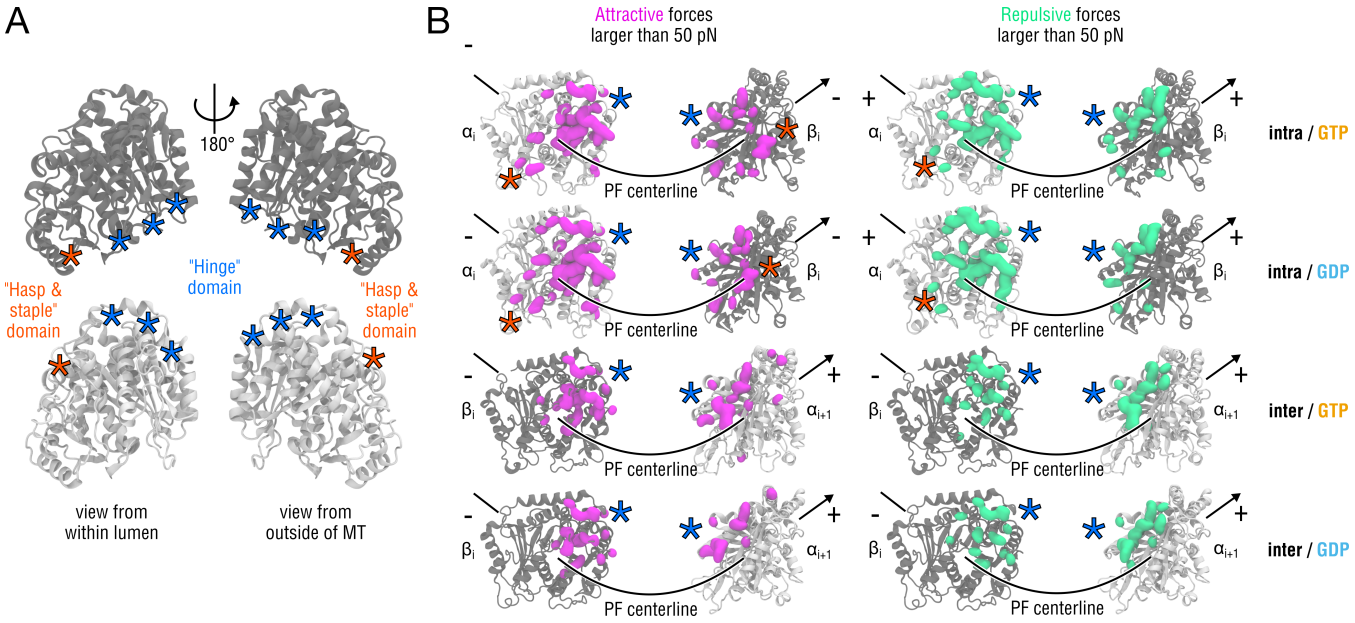

Fig. S5. (A) Schematic showing the location of key intra- and inter-dimer interaction domains termed 'hinges' (marked with red stars) and 'hasp & staple' (marked with blue stars). **(B)** Intra-dimer (two top rows) and inter-dimer (two bottom rows) contact clusters of pairwise interaction forces obtained by the Force Distribution Analysis (FDA). Amino acids contributing to attractive interactions (negative forces) are marked with magenta blobs, whereas those contributing to repulsive interactions (positive forces) are marked with green blobs. α- and β-tubulins are shown as silver and gray ribbons, respectively. The force distribution analysis was performed using a modified version of GROMACS 2020.4 that includes an implementation of the FDA module v2.10.2 (https://github.com/HITS-MBM/gromacs-fda). For the visual analysis of force distributions, forces between pairs of residues – located at intra- and inter-dimer interfaces – were calculated and averaged over the concatenated PF trajectories for each nucleotide state. A cutoff of 50 pN was applied to the absolute force values to highlight only strong clusters. For the purpose of analysis, solvent and KCl atoms as well as atoms involved in virtual site constraints were removed from the concatenated trajectories. Post-hydrolysis changes in the force distributions (Fig. 2*B,C*) were calculated by subtracting the average GTP distribution from the average GDP distribution and filtering out changes smaller than 50 pN and larger than -50 pN. These changes were then mapped onto the PF structures and color coded according to the sign of the changes.

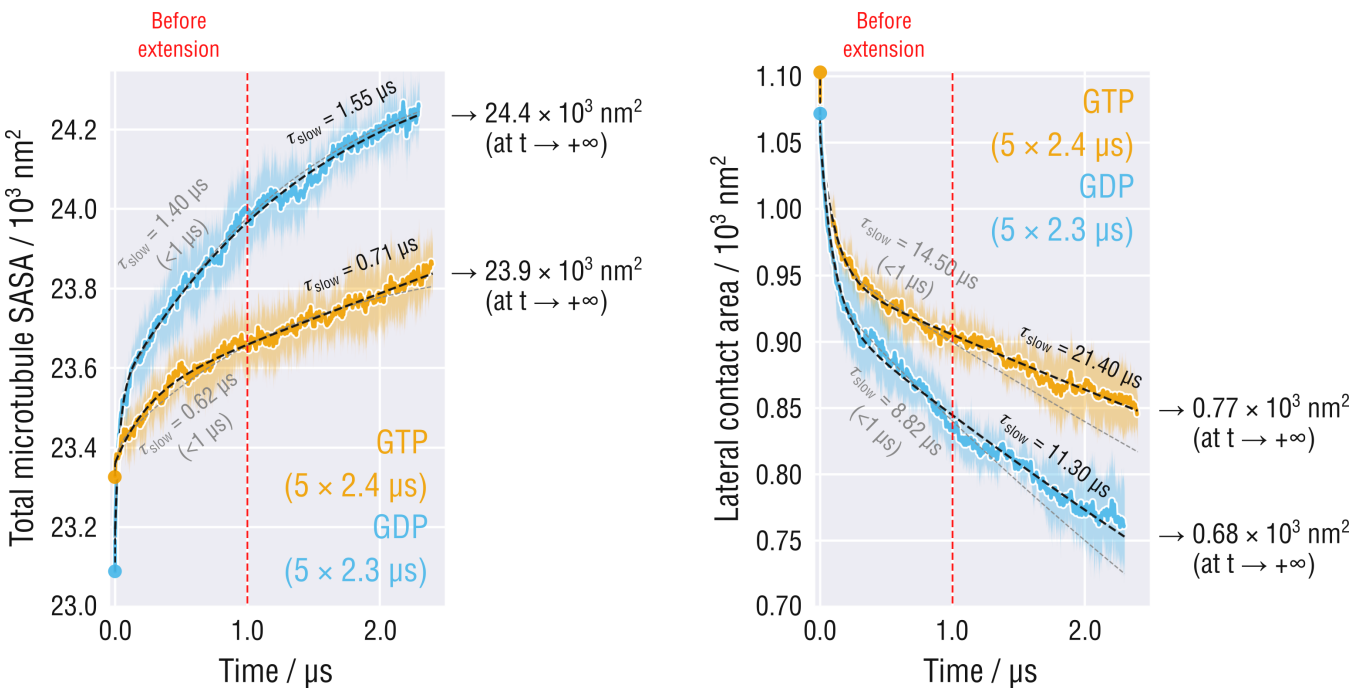

Fig. S6. Time evolution of the total MT SASA left and the lateral contact area (right) in the extended relaxation simulations. In both cases, the simulations were averaged over the five independent tip relaxation runs (same color coding as in Fig. 3 for GTP- and GDP-MTs was used). Black dashed lines depict fits with a two-component exponential decay function to the extended data. Gray dashed lines depict fits only to the first 1 μs of the runs. Characteristic decay times of the slow components are indicated as inserts. The MT relaxation trajectories were stored every 125000 steps (500 ps). The time-resolved MT SASA, $SASA_{MT}(t)$, was calculated using the memory-efficient internal GROMACS tool `gmx sasa`. The lateral contact area was expressed as a sum over the SASA of all PFs separately minus the total MT SASA divided by two, that is, $SASA_{lat}(t) = 1/2\left(\sum_{i=1}^{14} SASA_{PF_i}(t) - SASA_{MT}(t)\right)$.

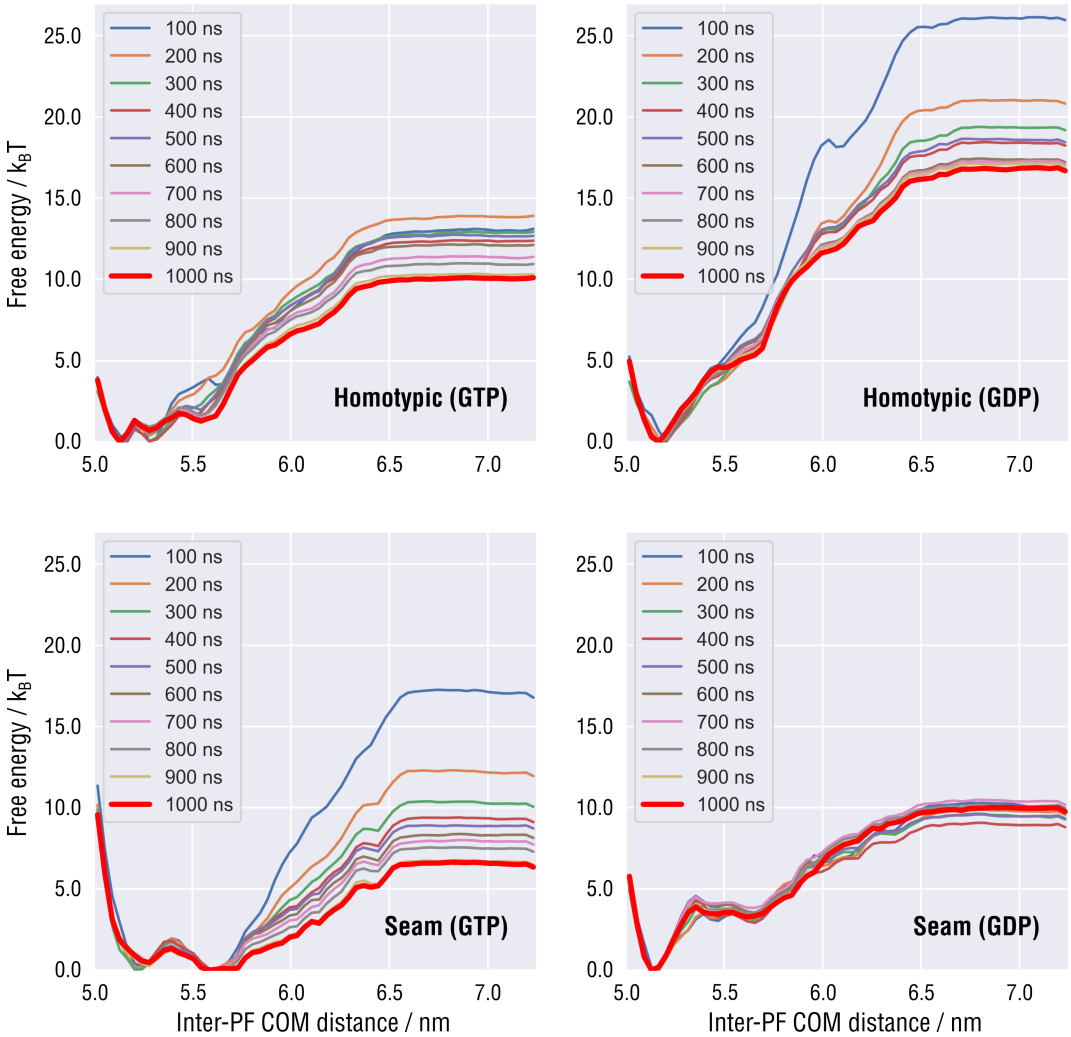

Fig. S7. Convergence of the lateral interaction free energy landscapes for both nucleotide states and contact topologies with the length of umbrella sampling trajectories taken for the analysis. Except for the one corresponding to the seam contact in GDP state (bottom right), all of the free energy landscapes initially overestimate the later interaction free energy and then gradually converge to the steady-state profiles as the amount of sampling increases. For the final profiles (red thick lines), the maximum deviation from the previous increment (900 ns per window) is less than 1 k_BT.

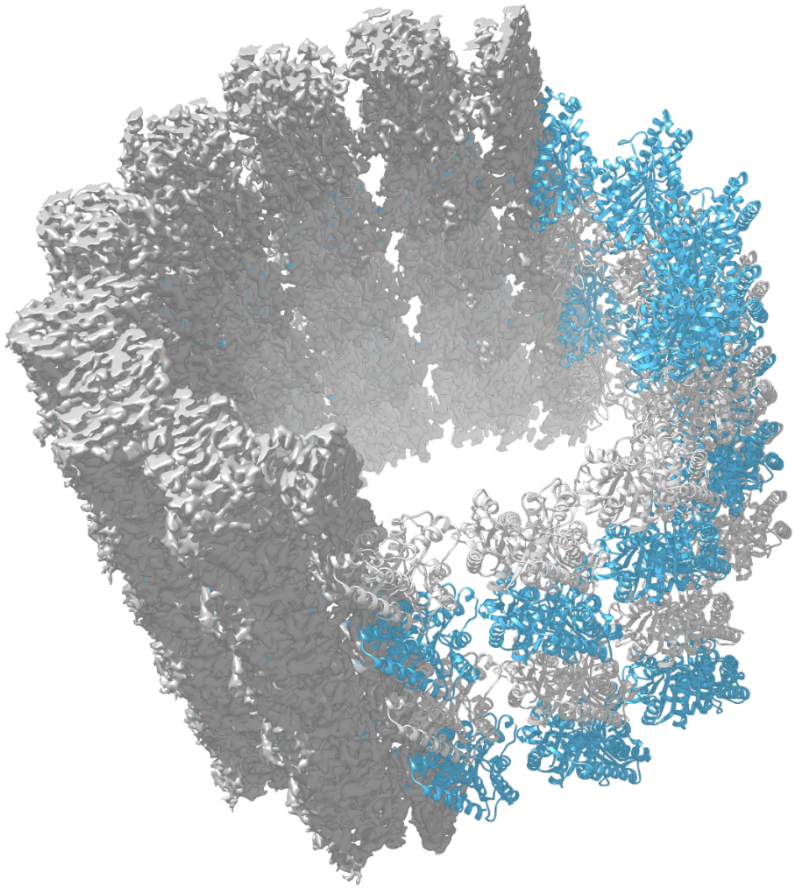

Fig. S8. Shown is the cross-section of the cryo-EM map section used in the refinement simulation filled with rigid-body fitted copies of the atomistic dimer model.

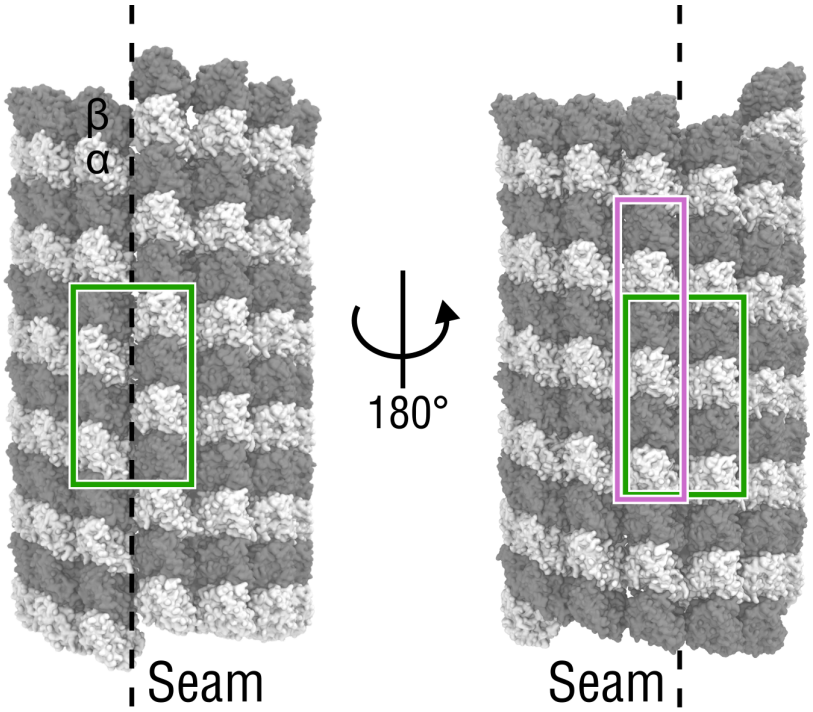

Fig. S9. Locations of the part of the full MT tip model used to extract the starting structure for the single-PF simulations (purple rectangle) as well as of the seam and seam-distant parts used to extract the 2×2 tubulin patches for the umbrella sampling simulations of lateral PF-PF interactions (green rectangles).

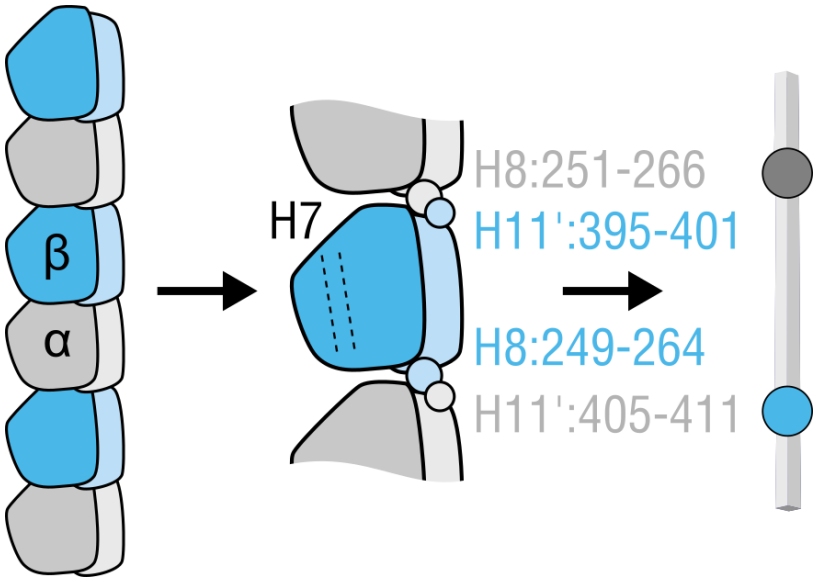

Fig. S10. Schematic illustrating the definition of a PF trace. PF traces were calculated to analyze the deflections of individual PFs in a radial plain passing through the MT central axis and an azimuthal plane orthogonal to the MT central axis. To this end, a discrete contour was drawn on each PF structure using specific reference points, here referred to as *nodes*. The definition of the nodes depended on the type of the longitudinal contact (*i.e.*, intra-dimer or inter-dimer) as well as on the position of the tubulin dimer in the PF (*i.e.*, terminal or non-terminal). For each non-terminal intra-dimer interface, the node was defined as the center-of-mass of the residues α:405-411 and β:249-264. For each non-terminal inter-dimer interface, the center-of-mass of α:251-266 and β:395-401 was used. The residues α:251-266 and β:395-401 were used to define the minus- and plus-end nodes, respectively.

Movie S1. Visualizations of the relaxation process of the simulated GTP- and GDP-MT tips. Top view from the MT plus-end.

Movie S2. Visualizations of the relaxation process of the simulated GTP- and GDP-MT tips. Side view facing the seam.

Movie S3. Visualizations of the twist-bending and tangential 'swing' modes of PF motion. For each mode, a top view and a side view were recorded.

SI Dataset S1 (MT_GTP.txt)
Atomic coordinates of the initial GTP-MT tip models in the PDB format.

SI Dataset S2 (MT_GDP.txt)
Atomic coordinates of the initial GDP-MT tip models in the PDB format.